Remote Sens. **2014**, *6*, 4515-4545; doi:10.3390/rs6054515

OPEN ACCESS

remote sensing

ISSN 2072-4292

www.mdpi.com/journal/remotesensing

Article

Evaluating the Potential of WorldView-2 Data to Classify Tree Species and Different Levels of Ash Mortality

Lars T. Waser [1,*], Meinrad Küchler [2], Kai Jütte [3] and Theresia Stampfer [3]

[1] Landscape Dynamics, Swiss Federal Research Institute WSL, Birmensdorf 8903, Switzerland

[2] Biodiversity and Conservation, Swiss Federal Research Institute WSL, Birmensdorf 8903, Switzerland; E-Mail: kuechler@wsl.ch

[3] Landesforst Mecklenburg–Vorpommern, Betriebsteil Forstplanung, Versuchswesen, Informationssysteme, Fachgebiet 033 Entwicklung und Betrieb IT-gestützter Fachverfahren, Schwerin 19061, Germany; E-Mails: Kai.Juette@lfoa-mv.de (K.J.); Theresia.Stampfer@lfoa-mv.de (T.S.)

***** Author to whom correspondence should be addressed; E-Mail: waser@wsl.ch; Tel.: +41-44-739-2292.

Received: 12 March 2014; in revised form: 4 May 2014 / Accepted: 7 May 2014 / Published: 16 May 2014

Abstract: Forest disturbances in central Europe caused by fungal pests may result in widespread tree mortality. To assess the state of health and to detect disturbances of entire forest ecosystems, up-to-date knowledge of the tree species diversity is essential. The German state Mecklenburg–Vorpommern is severely affected by ash (*Fraxinus excelsior*) dieback caused by the fungal pathogen *Hymenoscyphus pseudoalbidus*. In this study, species diversity and the magnitude of ash mortality was assessed by classifying seven different tree species and multiple levels of damaged ash. The study is based on a multispectral WorldView-2 (WV-2) scene and uses object-based supervised classification methods based on multinomial logistic regressions. Besides the original multispectral image, a set of remote sensing indices (RSI) was derived, which significantly improved the accuracies of classifying different levels of damaged ash but only slightly improved tree species classification. The large number of features was reduced by three approaches, of which the linear discriminant analysis (LDA) clearly outperformed the more commonly used principal component analysis (PCA) and a stepwise selection method. Promising overall accuracies (83%) for classifying seven tree species and (73%) for classifying four different levels of damaged ash were obtained. Detailed tree damage and tree species maps were visually inspected using aerial images. The results are of high relevance for forest

managers to plan appropriate cutting and reforestation measures to decrease ash dieback over entire regions.

Keywords: ash dieback; variable selection; multispectral remote sensing; object-based image analysis; remote sensing indices; tree species; tree mortality

1. Introduction

In-depth knowledge on tree species diversity and tree mortality is required to assess disturbances and state of health of forest ecosystems and to perform monitoring and protection tasks. Widespread tree damage can be caused by hurricanes, insects or fungal pests, which are the most significant disturbances to forest ecosystems in central Europe [1]. They have increased recently due to human impact and climate change [2].

Recent severe tree damage in the German state Mecklenburg–Vorpommern is caused by the fungal pathogen *Hymenoscyphus pseudoalbidus* and has expanded rapidly over the last few years in the northern part. It is currently ravaging trees in Europe, killing *Fraxinus excelsior* and *Fraxinus angustifolia* trees of all age classes [3]. Ash trees are important locally not only from an economic perspective, but also from an aesthetic one; they are also valuable for biodiversity. Both the immediate impact and the long-term consequences of the disease on the forest ecosystems in the disturbed areas are likely to be serious. Thus, an assessment of the extent of ash damage is required for evaluating the possible impact on tree species diversity in this area.

Assessing forest disturbance is mainly based on analyses of changes in chlorophyll content, leaf water content, and detection based on structural changes in damaged forests. The detection of gaps, deadwood or tree mortality has been carried out using optical airborne data e.g., [4,5] or spaceborne data e.g., using RapidEye [6], Quickbird [7–9] and IKONOS [10]. Airborne laser scanning (ALS) has been used to map live and dead forest biomass [11], to detect defoliation [12] and mortality [13] of coniferous trees. A general overview of the existing approaches for assessing impacts on aboveground biomass and canopy structure is given in [14].

These studies all show that it is now feasible to detect areas with tree mortality, in particular distinguishing between healthy and dead trees. To estimate the severity of forest disturbances, multiple levels of tree damage or tree mortality at the individual tree level are required. For example, multispectral digital aerial images have been used to detect multiple levels of coniferous tree mortality [4], hyperspectral technology to assess various levels of ash decline [15], or to map bark beetle-induced tree mortality [16], and multitemporal Quickbird and WV-2 data to quantify tree mortality of pinyon-juniper woodland [17]. Tree mortality resulting from insect outbreaks was assessed using multitemporal Landsat data in combination with multitemporal indices, e.g., enhanced wetness difference index (EWDI) [18,19]. Moreover, in [20,21] biophysical forest variables such as LAI and chlorophyll content obtained from image spectroscopy were successfully used to detect tree reflectance changes and tree stress. An overview of currently used techniques to detect tree mortality is given in [17]. However, to improve tree mortality detection, *i.e.*, by quantifying different levels of tree damage, additional spectral information besides the original bands of multispectral images is essential.

Meanwhile, several remote sensing indices (RSI) have been developed and successfully applied to fully explore vegetation covers. In many studies, the normalized difference vegetation index (NDVI), or variations thereof, are used as valuable damage indicators. For example, [4,7,9] have shown that NIR, NDVI and band ratios are appropriate for differentiating between live green trees that have turned red or gray after a pine beetle attack. However, there is a lack of studies aiming at the detection of multiple levels of tree damage in European forests due to human impacts and global warming.

During the past decade, considerable effort has been invested in assessing tree species diversity using high-resolution optical satellite data e.g., [22–25], digital aerial images e.g., [26], hyperspectral images e.g., [27], ALS e.g., [28], or aerial images in combination with ALS e.g., [29]. Contemporary new satellites such as WorldView-2 (WV-2) offer new perspectives as they have greatly increased geometric, radiometric, and spectral (up to eight bands) resolution for processing and analytic methods. According to, for instance, [30–32], the new spectral bands of WV-2 coastal blue, yellow, RedEdge and NIR2 enable gaps to be filled with detection of different types of vegetation such as tree species or tree mortality. Some recently published studies on tree species mapping used the eight bands of WV-2 data and produced promising results [33,34]. However, few attempts [25] have been made to classify tree species for the specific conditions of European forests using WV-2 data.

The use of very high spatial resolution (VHR) imagery poses a new methodological challenge, because the spectral response of an individual tree is influenced by variation in canopy illumination and background effects [34]. Using object-based image analysis (OBIA) may therefore be the best approach [25,35,36]. Besides modern machine learning algorithms (e.g., [16,25]), OBIA in combination with e.g., linear discriminant analysis (LDA) for feature selection [25] and regression techniques, such as e.g., generalized linear models (GLM) have proven to be particularly useful for assessing the spatial distribution of tree species based on remotely sensed explanatory variables [26,37–39]. GLMs enable easy and experienced feature selection procedures and model diagnostics, as well. Moreover, the growing need for sensitive tools to predict spatial and temporal patterns of species or communities is reflected by an increasing usage of predictive spatial modeling over the past 20 years [36,38].

The main focus of this study was to explore the potential of new WV-2 satellite imagery for semi-automatically classifying tree species and multiple levels of damaged ash in a German study area. Both classification approaches use *a priori* information from a forest data base and aerial image interpretation as reference data, and include OBIA in combination with multinomial logistic regression models. We therefore explored and compared: (1) the use of original WV-2 image bands; (2) the additional use of existing RSIs and the development of new indices to detect different levels of damaged ash; and (3) the production of area-wide detailed tree damage and tree species maps. These maps shed light on dynamics in stand structure and how species diversity may be affected by tree mortality. Our study demonstrates the potential of RSIs derived from eight band WV-2 data in distinguishing multiple levels of damaged ash. The transferability of the developed methods to other regions, pros and cons of the reference data sampling method, alternative sensors and the ideal time of image acquisition are also discussed.

2. Material

2.1. Study Area

Mixed forest areas in the German state Mecklenburg–Vorpommern close to Schuenhagen (54°15′N, 12°50′E) were selected as a test site for this study, covering approx. 60 km^2. The selection was based on the requirements by the forest department and the availability of detailed reference information on damaged ash. Geographically, the study area belongs to the Baltic coast (Figure 1), with an elevation ranging from 70 to 100 m above sea level. The climate is continental with an average precipitation of around 700 mm per year and a mean annual air temperature of around 8.5 °C, with daily means of 0 °C in January and 18 °C in July. Forests cover approximately 40%, and the rest is used for agriculture (crops and pastures) and settlements.

Figure 1. Location (**left**) and WorldView-2 scene (**right**) of the study area Schuenhagen in the German state Mecklenburg–Vorpommern.

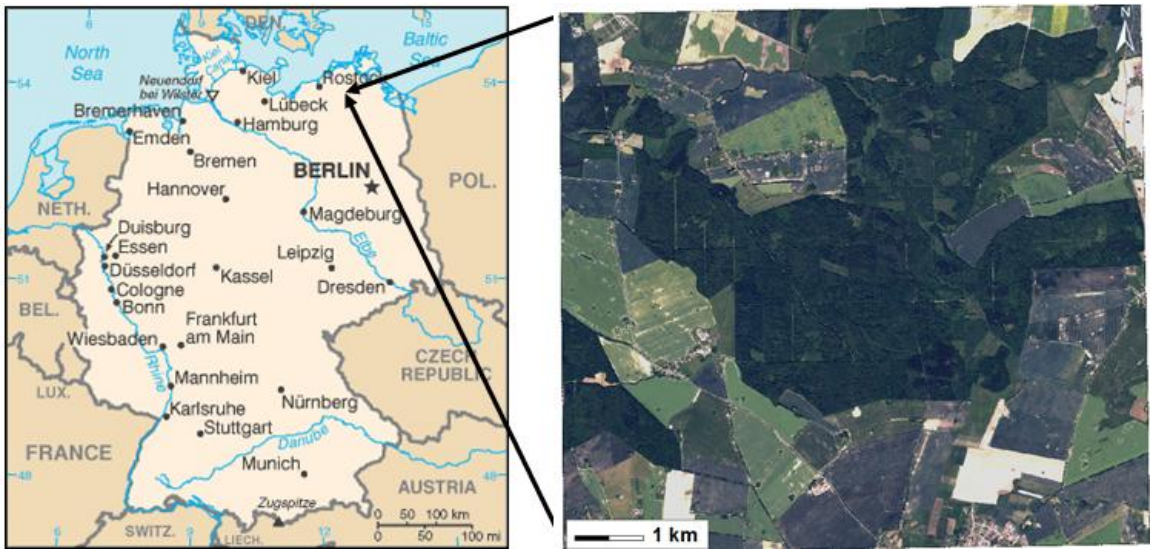

The forest is highly diverse and has a heterogeneous species composition, with many different age classes and multilayered stands. The dominant tree species are: ash (*Fraxinus excelsior)*, beech (*Fagus sylvatica)*, Douglas fir (*Pseudotsuga menziesii*), larch (*Larix decidua*), Norway spruce (*Picea abies*), poplar (*Populus sp.*) and oak (*Quercus pedunculata*).

2.2. Remote Sensing Data

2.2.1. WorldView-2 Image and Preprocessing

High spatial resolution digital imagery was acquired on 4 June 2011 from a WV-2 satellite. The satellite scene was ordered as multispectral (MS) and panchromatic (PAN) with spectral information coded in units of digital numbers (DN). The main sensor specifications are given in Table 1.

Table 1. Technical specifications of the WV-2 imagery.

Sensor Specifications	
Data acquisition	Study area 1: 4 June 2011 10:25:18 UTC
Spectral Resolution [nm]	Panchromatic: 450–800 Coastal: 400–450 Blue: 450–510 Green: 510–580 Yellow: 585–625 Red: 630-690 RedEdge: 705–745 NIR1: 770–895 NIR2: 860–1040
Spatial Resolution	0.5 m PAN and 2.0 m MS
Radiometric Resolution	11 bits per pixel

Since the single usage of dehazing and in combination with atmospheric correction (*ATCOR 2)* produced many artifacts in the forest parts, only the original multispectral image was pan-sharpened by fusing the coarse spatial resolution data with the higher spatial resolution panchromatic band using the modified IHS (intensity, hue, saturation) resolution merge algorithm [40]. Then, the 0.5 m pan-sharpened multispectral image was orthorectified using a 5 m digital terrain model (DTM). The coordinates of the control points were taken from an orthoimage (recorded in summer 2011, 0.5 m pixel size) resulting in a RMSE of 0.8 pixels on the 0.5 m WV-2 imagery. The pan-sharpened WV-2 image served as a basis for all investigations of this study.

2.2.2. Digital Aerial Images

A set of Nikon D300s RGB/CIR aerial stereo-images was used as a reference to delineate the crowns of damaged ash (Table 2) and the seven tree species (Table 3). The 8-Bit aerial images were acquired on 10 July 2011 by State Forest Department of Mecklenburg–Vorpommern using a Comco Ikarus C42 aircraft. The images have a side overlap of 80%–90% and 30%–60% between strips and include three visible bands and one near-infrared band at a 0.2 m spatial resolution.

2.3. Reference Data

2.3.1. Damaged Ash

Ash dieback has rapidly expanded in recent years in the northern part of Mecklenburg–Vorpommern. *Fraxinus excelsior* is being killed by *Hymenoscyphus pseudoalbidus*, which is a virulent fungal pathogen that attacks ash trees and causes "chalara ash dieback" (see e.g., [41]). The pathogen affects the bark, crown, branches and leaves, and causes different levels of leaf loss, crown dieback, and also a certain degree of leaf discoloring. It usually leads to tree death. Reference data to assess ash damage was collected in two steps.

First, 385 differently damaged individual ash trees belonging to the upper story were selected from the data storage forest (DSW-2) (see Table 2). The DSW-2 is an information system with a database from the three German states Mecklenburg–Vorpommern (present study), Brandenburg and Thüringen with information on the current state of the forest, data for future forest planning and management, and the effectiveness of management measures. It is managed by the three state forest departments and consists of over 200 different tree and forest parameters that are continuously updated; relevant for this study were tree species and health (ash mortality).

Table 2. Levels 1–4 of damaged ash with the number of digitized polygons and image segments. The assessment is based on the overall crown condition. Number of polygons are the delineated reference polygons, whereas the number of segments are the corresponding segments in the WV-2 orthoimage.

Damage Level	% Damaged	Characteristics	Number of Delineated Polygons	Number of Assigned Image Segments
1	<25	slight decline (<25% of crown damaged)	105	109
2	25–<50	moderate decline (<50% of crown damaged)	90	92
3	50–<75	moderate—severe decline (>50% of crown damaged)	88	91
4	75–100	severe decline (>75% of crown damaged)	102	107
∑ samples			385	399

Second, the corresponding sunlit tree crowns of the selected ashes from the DSW-2 records were delineated on the Nikon D300s RGB/CIR stereo images. Due to the time gap between these records and the aerial images (up to several months), the degree of damage had to be manually checked. Thus, each delineated ash crown was thoroughly inspected on the aerial images by experts. For each ash crown, density was estimated and the resulting damage level was checked and, if necessary, adapted. The visual inspection of different levels of damaged tree crowns was done on the base of false-color aerial images. The crowns of non-damaged ash appear in bright red colors whereas slightly damaged tree crowns are pink and heavily damaged are gray (Figure 2). Since damage rating is based on an assessment and quantification of the condition of canopy, *i.e.*, the percentage of crown decline and transparency, expert knowledge of the correlation of tree mortality and crown densities was essential. Thus, to train and recheck the entire interpretation of the ash damages, 60 randomly selected and differently damaged ash trees were additionally visited in the field by experts and by the local foresters and also inspected from above using a mobile crane. Ash damage was separated into four levels, ranging from: (a) level 1 trees with slight damage (<25% of crown damaged); (b) level 2 trees with moderate damage (25%–<50% of crown damaged); (c) level 3 trees with moderate to severe damage (50%–<75% of crown damaged); to (d) level 4 trees with severe damage (75%–100% of crown damaged). Level 4 trees with 100% destroyed foliage were much rarer since they had mostly been removed by the foresters. An overview and the criteria for the damaged ash are given in Table 2.

Examples of the four damage levels are given in Figure 2, and delineated crowns on the WV-2 orthoimage are illustrated in Figure 3.

Figure 2. Examples of the four different levels: (**a**) (<25%); (**b**) (25%–<50%); (**c**) (50%–<75%): and (**d**) (>75%) (clockwise) of damaged ash. Parts of the crane used for the training is visible in the right upper image.

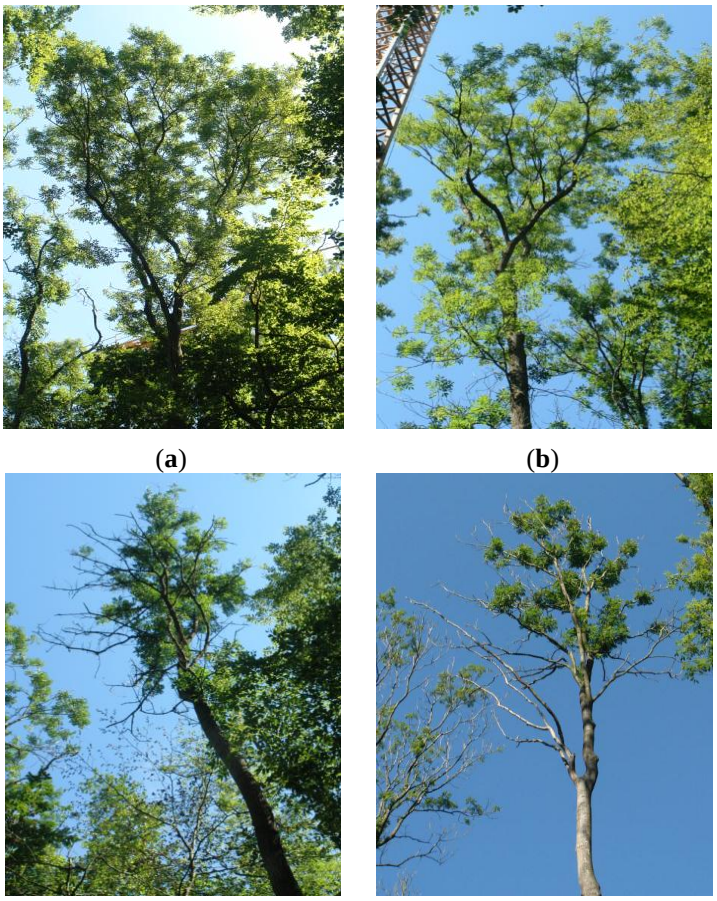

Figure 3. Example of delineated tree damage (levels 1–4) for ash using the CIR aerial images. Slightly damaged crowns of ash appear pink (1) and heavily damaged ones gray (4).

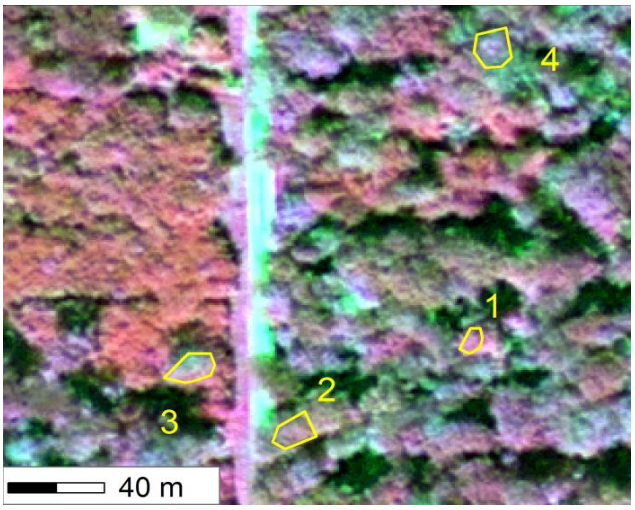

2.3.2. Tree Species

In addition to the damaged ash trees, reference data for six other tree species (beech, larch, Norway spruce, poplar, Douglas fir and oak) was collected based on the DSW-2 information (tree position and species code) and a delineation of the correspondingly sunlit tree crowns (in total 995) using the Nikon D300s RGB/CIR stereo images. Assigning the correct species code (from the DSW records) was not problematic since each tree crown could be 100% identified. Possible time differences between the DSW-2 species information and the aerial images are not critical for species classification since the status of health was not assessed. The sample for ash is large since it consists of the previously selected ash trees (see Section 2.3.1). Table 3 gives an overview of the tree species included in this analysis. The focus was laid on the main tree species, which were selected by the forest department.

Table 3. Tree species sampled. Number of polygons are the delineated reference polygons, whereas the number of segments are the corresponding image segments in the WV-2 orthoimage.

Scientific Name	Common Name	Number of Delineated Polygons	Number of Assigned Image Segments
Fagus sylvatica	Beech	92	143
Fraxinus excelsior	Ash	385	399
Larix decidua	Larch	109	113
Picea abies	Norway spruce	105	105
Populus sp.	Poplar	121	128
Pseudotsuga menziesii	Douglas fir	82	104
Quercus pedunculata	Pedunculate oak	101	141
∑ samples		995	1133

3. Methods

The main steps in processing the input data are: (a) shadow masking; (b) image segmentation to extract individual tree crowns or clusters of trees; (c) assignment of reference data to image segments; (d) calculation of explanatory variables for each image segment; (e) selection and reduction of variables using three approaches; and (f) performing supervised classifications of each image segment (tree species and damaged ash). The methodological workflow is given in Figure 4.

3.1. Shadow Masking and Image Segmentation

Shadowed image pixels were excluded to guarantee that only sunlit tree crowns would be used in the classification approaches. The sunlit areas were separated using intensity values $I_{[RGB]}$ from an IHS-transformation of the RGB bands (5-3-2), where values smaller than 0.10 were assigned to shadows. The threshold was determined by first checking the histogram of the intensity image and based on visual inspection to separate shadowed and non-shadowed areas. Pixels belonging to this shadow mask were excluded from further processing steps.

Figure 4. Methodological workflow of the ash damage and tree species classification approach.

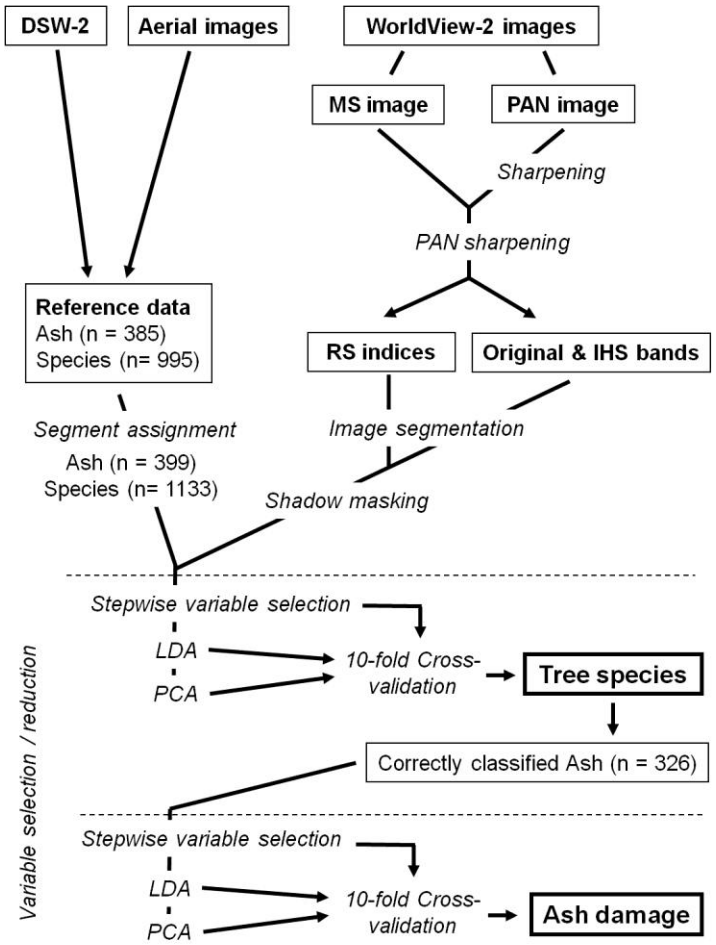

The sunlit WV-2 orthoimages were subdivided into patches through multiresolution segmentation using the *eCognition Developer 64 8.7* software [42,43]. The size of the objects was adjusted to the scale of the investigation (tree crowns and tree clusters) for each segmentation level. The optimal segmentation parameters depend on the scale and nature of the tree crowns to be detected, which differ considerably between coniferous and deciduous trees. The segmentation quality was therefore evaluated on the sunlit tree crown polygons of the reference data. Segmentation was iteratively optimized using several levels of detail and adapted to shape and compactness parameters until the crowns and segmented polygons became almost congruent. The final segmentation consists of 669,700 objects and yielded individual trees and tree clusters with similar shapes and spectral properties. The pan-sharpened WV-2 orthoimage was used as input dataset, with a scale parameter of 20, and homogeneity criterions of 0.7 for both shape and compactness.

3.2. Assignment of Reference Data to Segments

The aerial image-based crown delineations of the ash damage levels and the tree species were transformed to the WV-2 orthoimage, and their positions were all visually checked. However, since the crown delineations (polygons) from the aerial images were rarely congruent with the automatically generated segments of the WV-2 orthoimage, the corresponding image segments had to be selected manually. Then the damage or species code were assigned to each corresponding segment. Since the

tree crowns in the WV-2 orthoimage often consist of two or more image segments, the numbers of assigned crown segments (in Tables 2 and 3) are often larger than the delineated crown polygons of the reference data, especially for deciduous trees. In total, 399 segments of the four different levels of ash damage and 1133 segments of the seven tree species were assigned.

3.3. Explanatory Variables

A total of 33 variables were extracted from the WV-2 orthoimage and were calculated. For each image segment, both the mean and standard deviation of these variables were recorded resulting in 66 explanatory variables. Prior to variable selection, the variables were grouped into three sets: (1) the eight original multispectral WV-2 bands and six derivations from them; (2) the 19 (see Section 3.3.2) Remote Sensing Indices (RSI); and (3) all variables.

3.3.1. WV-2 Image Bands

The inclusion of RGB- and NIR-related explanatory variables is based on studies dealing with image processing [44–47]. The eight bands of the pan-sharpenedWV-2 orthoimage (Table 1) are used as the basic spectral variables. Additionally, the bands RGB and RGNIR1 were color transformed to IHS into the channels intensity (I), hue (H), and saturation (S) to separate the effect of illumination to the quantity of intensity. These six new variables are: $I_{[RGB]}$, $H_{[RGB]}$, $S_{[RGB]}$, $I_{[RGNIR1]}$, $H_{[RGNIR1]}$, and $S_{[RGNIR1]}$. Thus, 14 features were derived from the image bands. Including the means and standard deviations gives a total of 28 explanatory variables.

3.3.2. Remote Sensing Indices

Remote Sensing Indices (RSI) have been extensively used since the 1970s, according to [48], to explore vegetation's spectral signature characteristics, both in the visible and near-infrared part of the spectrum [49]. Implementing green channel-based indices has been found beneficial (e.g., [50]), as has RedEdge [51], and yellow and NIR2 (both WV-2) [32]. Many studies have focused on evaluating spectral indices in terms of their sensitivity to vegetation biophysical parameters, as well as to external factors affecting canopy reflectance [52]. Moreover, spectral RSIs have been widely adopted to monitor forest states and canopy processes, e.g., [48] for general forest applications, and [34] for tree species. A general overview of RSIs is given in the *ENVI* user's guide [53] of Exelis Visual Information Solutions and sensor specific by the [54].

The inclusion of 19 RSIs was mainly based on these studies, on ENVI, and on the visual analysis of the vitality of the damaged ash on the orthoimage. Empirical testing including histogram analysis and visual inspection revealed that RSIs based on the spectral bands green, red, RedEdge, NIR1 and NIR2 could detect different levels of tree mortality particularly well. Additionally, *in situ* spectral measurements on healthy and different levels of damaged ash were performed using a FieldSpec® HandHeld 2 in [55]. Based on the visual inspections and the spectral measurements, three additional RSIs were developed and empirically tested, including one with the blue band. Calculating the means and standard deviations, 38 explanatory variables were derived from these 19 RSIs. An overview of all RSIs used in this study is given in Table 4 [32,49,50,53,56–65].

Table 4. Applied remote sensing indices (RSI) adapted to the WV-2 bands in (band number in parentheses). B = Blue (2), G = Green (3), Y = Yellow (4), R = Red (5), RE = RedEdge (6), NIR1 = Near Infrared (7), NIR2 = Near Infrared (8).

Abbreviation	Name	Formula	Ref.
ARVI	Atmospherically Resistant Vegetation Index	(NIR1 − (R − (B − R)))/(NIR1 + (R − (B − R)))	[56,57]
DD	Difference Difference Vegetation Index	(2 × NIR1−R)−(G−B)	[58,59]
GI2	Greenness Index 2	(B × −0.2848 + G × −0.2434 + R × −0.5436 + NIR1 × 0.7243 + NIR2 × 0.0840) × 5	[32,50]
GNDVI	Green NDVI	(NIR1 − G)/(NIR1 + G)	[60]
NDRE	RedEdge NDVI	(NIR1 − RE)/(NIR1 + RE)	[61]
NDVI	Normalized Difference Vegetation Index	(NIR1 − R)/(NIR1 + R)	[49]
$NDVI_{3,5}$	Green–red ratio	(G − R)/(G + R)	[50]
$NDVI_{8,4}$	NIR-yellow ratio	(NIR2 − Y)/(NIR2 + Y)	[32]
NIRRY	NIR-Red-yellow ratio	(NIR1)/(R + Y)	[32]
NORM NIR	Normalized NIR	NIR1/(NIR1 + R + G)	[53]
PSRI	Plant Senescence Reflectance Index	(R − B)/RE	[62]
REY	RedEdge yellow ratio	(RE − Y)/(RE + Y)	[32]
RVI	Ratio Vegetation Index	NIR1/R	[58]
SA	Surface Albedo	((Y + R) × 0.35)/2 + (0.7 × (NIR1 + NIR2))/2 − 0.69	[63]
VI1	Vegetation Index based on RedEdge	(10,000 × NIR1)/$(RE)^2$	[64]
VIRE	Vegetation Index based on RedEdge	NIR1/RE	[65]
BR	Blue ratio	(R/B) × (G/B) × (RE/B) × (NIR/B)	self-developed
GR	Green–red ratio	G/R	self-developed
RR	Red ratio	(NIR1/R) × (G/R) × (NIR1/RE)	self-developed
∑ RSIs	19 (38 means and standard deviations)		

3.4. Variable Selection and Reduction

To reduce redundancy and intercorrelation among the 66 explanatory variables (66 = 19 means and 19 standard deviations of the RSIs, and 14 means and 14 standard deviations of the original WV-2 bands and IHS transformations), it was necessary to select the variables that contributed most prior to the object-based classification. Thus, a variable selection method was needed, which is fast, easy to reproduce, and requires only little additional arithmetic and processing effort. However, for practical data analysis, the function that should be used to fit the observed data is usually unknown (e.g., [66]). Many studies use familiar functions without knowing if they are better than other possible choices. According to [38,67], a small set of powerful variables has to be selected for the final model since a good fit to the given training data is not a sufficient condition for good predictive models.

In the first approach, variable selection is based on regression models (e.g., [68]) by minimizing Akaike's information criterion (AIC) [69]. As second and third approaches, linear discriminant analysis (LDA) and principal component analysis (PCA) are effective methods used to reduce variable space dimension and skip redundant and collinear variables; they have been successfully applied in, among others [25,29,47]. In the current study, these three techniques to select variables were tested using *R version 2.15.1* [70] and the GUI of *VEGEDAZ 2014* [71] where the *R* scripts are implemented.

3.4.1. Stepwise Variable Selection

Automated forward and backward stepwise selection (*R stats step*) was applied for each tree species and ash damage level, using all 66 explanatory variables. The algorithm minimizes within-class variance while maximizing the between-class variance for a given significance level. It is a combination of backward elimination (starting with all candidate variables and deleting all not-significant variables by testing them one by one) and forward selection (all variables are tested one by one if their contribution is significant after a new variable has been added) based on the AIC as reduction criterion with a level of significance $p < 0.01$ (for details, see [68–70]). If and how often a variable was selected by *R stats step* is shown in Tables A1 and A2.

3.4.2. Linear Discriminant Analysis

LDA (*R stats lda*) was applied on the three sets of the variables to reduce variable space dimension and thus redundancy and intercorrelation among the variables. LDA is a supervised statistical method, which allows a classification of the samples by analyzing a set of descriptors, (see e.g., [72,73]). It is typically used as a feature extraction step before classification. The aim is to find optimal discriminant vectors (transformation) by maximizing the ratio of the between-class distance to the within-class distance, thus achieving a maximum class discrimination. In the ideal case, it is a linear combination that completely separates the classes. However, in most cases, no transformation provides a complete separation of classes, thus the goal was to find the transformation that minimizes the overlap of the transformed distributions. The linear discriminants of all three subsets of variables were tested as explanatory variables for classifying tree species and ash damages (see Table A3).

3.4.3 Principal Component Analysis

PCA (*R stats prcomp*) was applied on three subsets of the variables. PCA involves a mathematical procedure that transforms a number of (possibly) correlated variables into a (smaller) number of uncorrelated variables called principal components. The first principal component accounts for as much of the variability in the data as possible, and each succeeding component accounts for as much of the remaining variability as possible. For details on the PCA see [74]. The PCA axis for all three subsets of variables, which explain >95% of the variance (cumulative proportion of all components) were tested as explanatory variables for classifying tree species and ash damages and best results are shown in (Tables A4 and A5).

3.5. Classification

Object-based approaches for both tree species and damage level classification were applied using multinomial logistic regression techniques as the response variables are polychotomous (for details, see [68]). Multinomial logistic regression is a simple extension of binomial logistic regression that allows more than two categories of the response variable where one (one species or damage level) is chosen as the comparison category. Separate relative risk ratios are determined for each category of the response variable with the exception of the comparison category, which is omitted from the analysis. The formula of the multinomial logistic regression function is given in Equations (1) and (2):

$$P(y_i = r) = \frac{\exp(X_i\beta_i)}{1 + \sum_{r=1}^{J}\exp(X_i\beta_r)} \quad (1)$$

and

$$P(y_i = 0) = \frac{1}{1 + \sum_{r=1}^{J}\exp(X_i\beta_r)} \quad (2)$$

where Y_i is the observed outcome for the *i*th observation on the response variable (one of the tree species), X_i is a vector of the explanatory variables (image bands, derivatives, and RSIs), and β_r is a vector of all the regression coefficients in the *r* th regression. β_i is the unknown coefficient estimates for the explanatory variables (estimated by maximum likelihood). *J* is the number of categories (1–7 tree species or 1–4 damage levels, respectively) and *r* is the damage level or tree species or damage level tested.

Like binomial logistic regression, multinomial logistic regression uses maximum likelihood estimates to evaluate the probability of categorical membership. Thus, the image segments were assigned to the species or damage levels, with the highest modeled probability. In *R version 2.15.1*, several functions for multinomial models are available. Of these, the *R* package *nnet* provides an implementation of multinomial logistic regression on the base of a neural network and is very robust with respect to redundant and collinear explanatory variables [75].

In the current study, the predictive power of the models using the explanatory variables provided by the three variable selection and reduction approaches was verified by ten-fold cross-validations. The statistical measures used to validate the classification results were: producer's and user's accuracy, overall accuracy (*OA*), and Cohen's kappa coefficient *(K)* (see e.g., [76,77]). According to [78], a value of ten for k-fold cross-validation is popular for estimating the generalization error and, according to [79], is preferable over leave-one-out cross-validation.

3.6. Predictive Mapping

Tree species maps and a map with the four different levels of damaged ash were produced for the entire extent of the WV-2 orthoimage showing the most probable classes if the modelled probability exceeded 90%. Since no external reference dataset was available, a visual quality control of the prediction for not-sampled trees was also applied. Thus, the seven predicted tree species and the four different levels of damaged ash were visually inspected using the Nikon D300s RGB/CIR aerial images.

4. Results

The accuracy assessment consists of both quantitative and qualitative aspects. The quantitative assessment was performed to categorize the delineated tree species and damaged ash polygons. The qualitative evaluation was carried out by visual inspection of the tree species and ash damage maps.

4.1. Classification Accuracy of the Seven Tree Species

Table 5 shows that best *OA* and *K* were obtained when a LDA was run on all 66 explanatory variables. Classifications based on LDA variables clearly outperform (10% higher *OA*) the stepwise selected variables and the variable selection based on PCA. Lowest accuracies were obtained when classification is based on stepwise selected variables. But the differences were smaller and not significant. The stepwise selection methods seem therefore least appropriate.

The statistical significance of the different classification accuracies based on the LDA and PCA was tested using the Wilcoxon rank sum test [80]. Each *OA* pair was chosen ten times randomly and independently. At the 0.05 significance level (*p-value*), the *OAs* yields of the WV-2 original bands and RSIs, and the RSIs and the combined variables were different.

Table 5. Overall accuracies (*OA*) for the seven tree species as obtained by different sets of explanatory variables and different selection approaches based on 1133 crown polygons. The best model is marked in bold.

Variable Selection and Reduction Approach	Variable Sets	7 Tree Species		
		OA	***K***	***p-value***
forward and backward stepwise	all	0.661	0.602	-
LDA	original bands and IHS	0.765	0.673	-
	RSIs	0.778	0.689	0.001
	all	**0.829**	**0.788**	**0.001**
PCA	original bands and IHS	0.738	0.628	-
	RSIs	0.761	0.661	0.001
	all	0.772	0.731	0.001

The confusion matrix in Table 6 summarizes the results of classifying the seven tree species using the classification model (based on the LDA of all variables) with best *OA* and *K*.

The best agreements (highest producer's accuracies) were obtained for poplar (95%), Norway spruce (92%), and Douglas fir (86%). Lowest accuracies were obtained for beech trees (69%), which are often misclassified as ash. Ash is often misclassified as one of the other deciduous trees (beech, oak) and less with poplar and coniferous trees. Larch trees (80%) were frequently misclassified as Norway spruce or Douglas fir.

Table 6. Confusion matrix for tree species classification with the producer's and user's accuracy of the classified tree segments of different tree species (n = 1133), *OA*, and *K*.

Reference Data	**Classified As**								
	Ash	**Beech**	**Oak**	**Poplar**	**Douglas Fir**	**Larch**	**Norway spruce**	∑	***Prod.'s Accuracy***
Ash	**326**	42	18	6	3	2	2	399	0.82
Beech	39	**99**	3	2	0	0	0	143	0.69
Oak	12	6	**117**	6	0	0	0	141	0.83
Poplar	4	2	1	**121**	0	0	0	128	0.95

Table 6. *Cont.*

Reference Data	**Classified As**								
	Ash	**Beech**	**Oak**	**Poplar**	**Douglas Fir**	**Larch**	**Norway spruce**	∑	***Prod.'s Accuracy***
Douglas fir	4	0	0	0	**89**	9	2	104	0.86
Larch	2	0	0	0	10	**90**	11	113	0.80
Norway spruce	2	0	0	0	3	3	**97**	105	0.92
∑	389	149	139	135	105	104	112	**939**	
User's accuracy	0.84	0.66	0.84	0.90	0.85	0.87	0.87	1,133	
OA	**0.83**								
K	**0.79**								

4.2. Classification Accuracies of Different Levels of Damaged Ash

Table 7 shows that the best *OA* and *K* were obtained when a LDA was run on all 66 explanatory variables. Classifications based on LDA variables clearly outperform the stepwise selected variables and the variable selection based on PCA. The classification performances and differences substantially increase if all RSIs are used instead of the single usage of original bands and IHS. The different levels of damaged ash were classified with around 30% lower accuracies when stepwise-selected variables are used. Both the stepwise selection methods and the PCA seem particularly weak.

Table 7. Overall accuracies (*OA*) for the four different levels of damaged ash based on the different sets of explanatory variables and 326 crown polygons. The best models are marked in bold.

Variable Selection and Reduction Approach	**Variable Sets**	**4 Damage Levels**		
		OA	***K***	***p-value***
Forward and Backward Stepwise	all	0.571	0.475	-
LDA	original bands and IHS	0.573	0.434	-
	RSIs	0.741	0.641	0.001
	all	**0.773**	**0.697**	**0.001**
PCA	original bands and IHS	0.468	0.292	-
	RSIs	0.558	0.488	0.001
	all	0.592	0.501	0.001

The statistical significance of the different classification accuracies based on the LDA and PCA was tested using the Wilcoxon rank sum test of the *OA*s. Each *OA* pair was independently and randomly chosen ten times. At the 0.05 significance level (*p-value*), the *OAs* yields of the WV-2 bands and the RSIs, and the RSIs and combined variables from both differed.

The confusion matrix in Table 8 summarizes the results of classifying damaged ash (Table 7) using the models (based on the selected variables suggested by LDA) with the best *OA* and *K*.

The best agreements (83%) were obtained for damage level 1 (<25% destroyed foliage), followed by damage levels 4 (80%) and 3 (76%). Damage level 2 (71%) had the lowest agreements. Misclassifications occurred particularly in damage levels 1 and 3, with less in level 4. Misclassification

of damage level 3 occurred in damage level 2 and 4, less in level 1. In contrast, damaged ashes belonging to level 4 are mostly confused with damage level 3.

Table 8. Confusion matrix for the classification of damaged ash with the producer's and user's accuracy of the classified tree segments of different ash damages (n = 326), *OA*, and *K*.

Reference Data	**Classified As**					
Ash Damage Level	**1 (<25%)**	**2 (<50%)**	**3 (<75%)**	**4 (<100%)**	∑	***Prod.'s Accuracy***
1 (<25%)	**64**	11	2	0	77	0.83
2 (<50%)	12	**60**	8	5	85	0.71
3 (<75%)	3	6	**58**	9	76	0.76
4 (<100%)	3	6	9	**70**	88	0.80
∑	82	83	77	84	**252**	
User's accuracy	0.78	0.72	0.75	0.83	326	
OA	**0.77**					
K	**0.70**					

4.3. Predictive Mapping

In a GIS, the predicted tree species map based on the classification model producing the highest overall accuracies (see Table 6) was visually inspected and compared with the WV-2 orthoimage and also with the corresponding Nikon D300s RGB/CIR aerial images. Special attention was paid to forest borders, clearings and to dense forest parts. The inspections at well-known locations confirm that the seven tree species are generally well classified. In Figure 5 examples of reference crown segments are given. The classified and mapped tree species of this subset are shown in Figure 6.

Figure 5. WV-2 CIR orthoimage (histogram-equalized) with reference crown segments of four different damage levels and three tree species. Shadows are masked out. The color of ash crowns (in the middle of the orthoimage) varies mostly due to different levels of ash mortality.

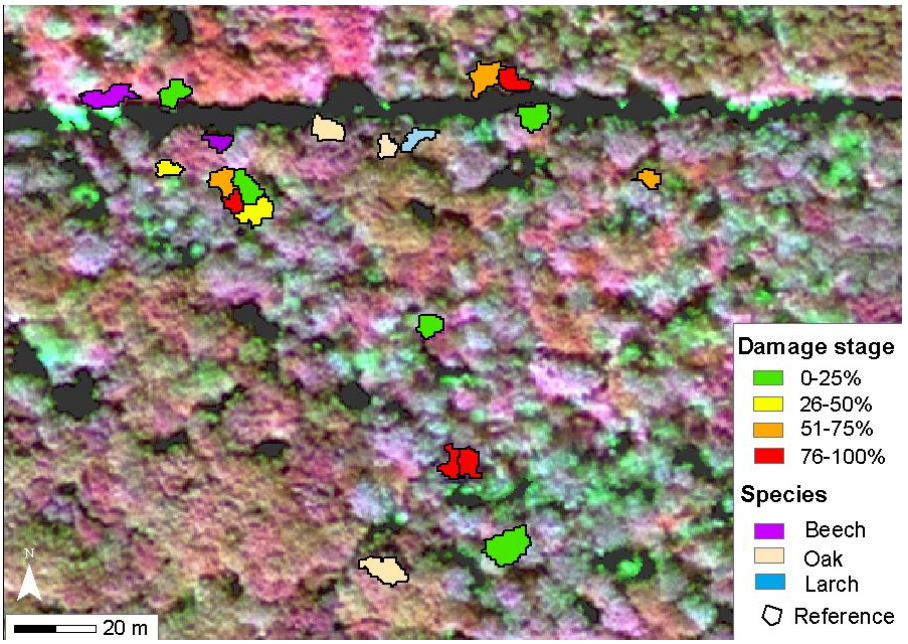

Figure 6. Subset of the corresponding tree species map with the selected reference crown segments. Shadows are masked out.

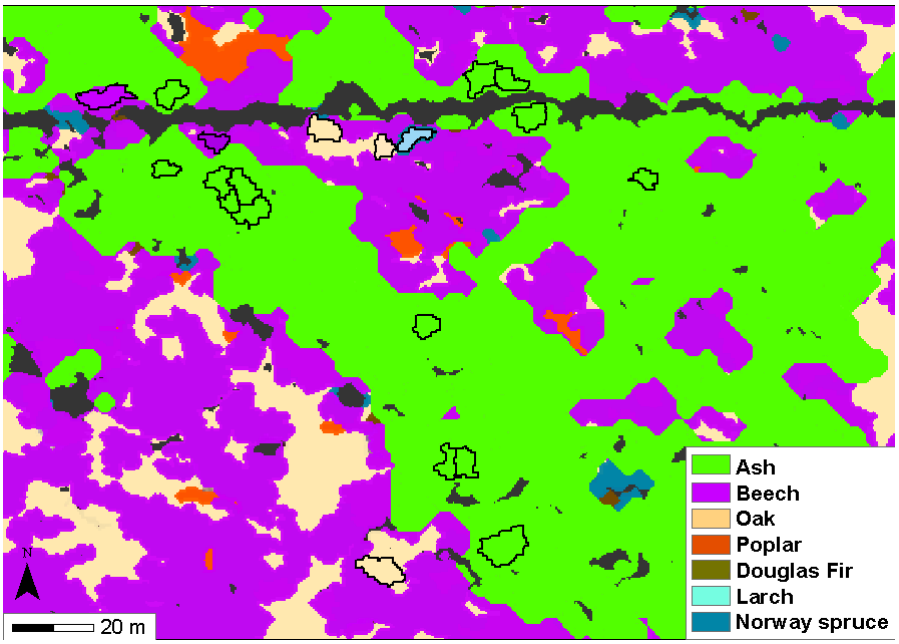

Figure 7. Subset of correspondingly damaged ash. Reference polygons are given for all four damage levels. The two falsely predicted segments are marked in blue. Shadows are masked out.

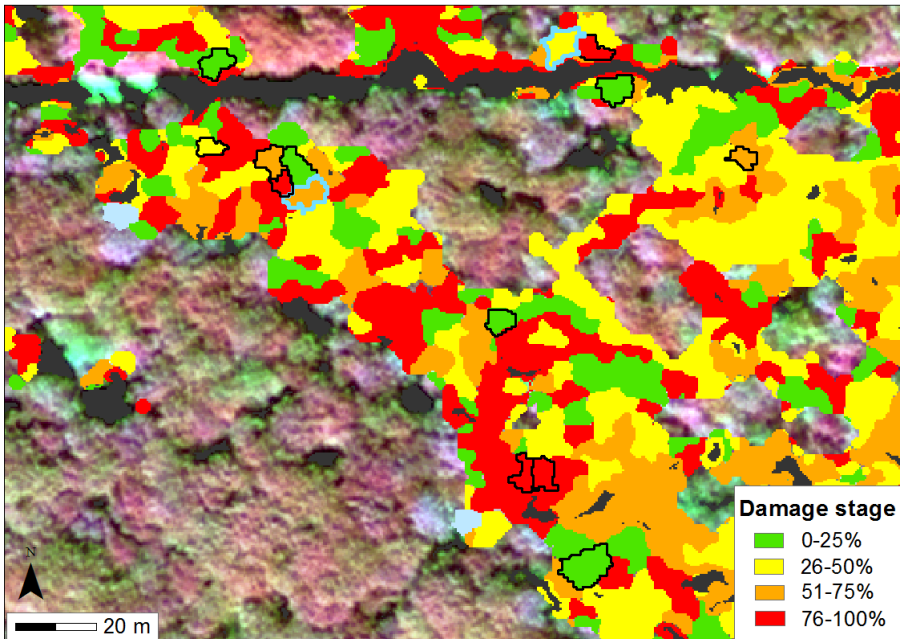

Figure 6 shows the dominance of ash, followed by beech and oak. All reference crown segments were correctly classified. The classification of ash seems reasonable; poplar and larch are also well detected. It seems that few small poplar segments (red) are confused with beech.

In addition to the tree species map, the predicted damages of ash based on the classification model producing highest overall accuracies (see Table 8) were also visually inspected and compared with the WV-2 orthoimage and also with the corresponding Nikon D300s RGB/CIR aerial images.

The inspections confirmed that the damage levels 1 (<25% destroyed foliage), also 3 (50%–<75%) and 4 (75%–100%) are generally well classified when using the LDA of both the image bands and the RSIs as explanatory variables. Problems mainly occur when classifying damage level 2 (25%–<50%), where segments are more often misclassified as damage level 1 and level 3, though less as level 4. Thus, damage level 2 seems to have a higher in-class variance, but also to be rather similar to each other, possibly due to the slight under- or overestimation of the stereo-interpretation of the sampling, as discussed below. Examples of the mapped ash are given in Figure 7.

5. Discussion

5.1. Classification Accuracies

The study reveals that WV-2 satellite data are highly suitable to separate seven tree species and four different levels of damaged ash. The achieved overall accuracies ranged between 83% for the seven tree species and 77% for four different levels of damaged ash.

Errors in the tree species classification were mainly related to ash, beech, and larch. Whereas confusion mainly occurs between the deciduous tree species ash and beech, larch was often misclassified as Douglas fir or spruce. Crown segments of differently damaged ash and healthy beech seem particularly difficult to separate. The classification results reveal that the detection of the four different levels of damaged ash was challenging and class assignment in some cases more difficult. Analysis of the histograms of the selected ash crown segments in the WV-2 orthoimages revealed that damage level 2 (destroyed foliage 25%–<50%) varied most. Our results confirmed this finding since damage level 2 was particularly often confused with damage levels 1 and 3, and less with 4. The most probable reasons for these misclassifications are the similar spectral properties of a few sample crowns among the tree species, and also among the different damaged ash and other species. Less probable, but theoretically possible, are mixed crown segments from a neighboring tree of a different species or different level of damage. Visual inspection of the classification maps confirmed that few small crown segments might be confused with neighboring segments, which belong to a different and more dominant tree species (e.g., for poplar in Figure 6).

The identification of seven different tree species in the WV-2 orthoimage incorporated ash with a varying mortality level. Thus, compared to the other tree species, the ash sample was relatively large (n = 399) and characterized by a high in-class variance. Besides this, there are other effects that can lead to misclassification of tree species, as well. For example, spectral variability can be considerable even within healthy tree species because of differences in illumination, the openness of the trees, shadowing effects and crown health, as well as natural variability. Another aspect is the fact that the spectrum of a tree species may change not only during the growing season but with tree age.

These uncertainties related to the different levels of tree damages make statistical evaluations more difficult. Overall, the accuracies obtained for the seven tree species are in line with or higher than those reported in comparable studies, but a direct comparison is difficult because: (1) higher accuracies are obtained with fewer or different classes and when inappropriate or no cross-validation is applied; (2) classification is based on other sensors; and (3) the forest structure, composition and health (usually no mortality) are different. For a good overview of studies on tree species classification

accuracy within the last ten years, see [25] for both airborne and spaceborne sensors and [47] for airborne sensors. Research by [25] showed 82% overall accuracy when classifying ten tree species in a European study using WV-2 data, and [81] obtained 77% overall accuracy when classifying seven tree species using IKONOS images. Seven tree species were classified by [34] in urban areas using IKONOS or WV-2 imagery with overall accuracies up to 68%.

Errors in the classification of different damage levels were mainly related to ash damage level 2 (25%–<50% destroyed foliage), which was quite often misclassified as damage levels 1 or 3. However, direct comparisons with other studies are difficult since most studies only classify living and dead trees without further distinction. If different levels of damage or mortality are not distinguished, overall accuracies are usually higher. For example, [17] identified living and dead tree pixels of pinyon-juniper woodlands based on Quickbird and WV-2 images with 98% overall accuracies. Hyperspectral imagery was used by [16], which obtained high overall accuracies between 84 and 96% for detecting dead spruce, and separation between the healthy trees and the dead trees with a 94%–97% accuracy. Three different levels of tree mortality, *i.e.*, green, red and gray trees were distinguished by [4]. The obtained producer's accuracies vary between 86 and 89%—albeit including other land cover classes—and are based on spatially aggregated 2.4 m aerial imagery. Alternatively, overall accuracies of 84% for different levels of defoliation were obtained by [12] using first/last pulse ALS data. As long as models of the same datasets are compared, the results can be interpreted as in this study. However, comparisons with other studies or transferability to other regions should be handled with care and, to be on the safe side, be interpreted as qualitative.

5.2. WorldView-2 Data and Pre-Processing

The suitability of WV-2 data has been thoroughly tested in this study and was confirmed by the high overall accuracies of the results. Besides the high spectral and radiometric resolution, another advantage is the appropriate spatial resolution of the sensor. In many classification studies, according to [22], complications with increased spectral variability arise when the spatial resolution becomes too fine, e.g., when using aerial images.

In this study, no atmospheric correction and dehaze reduction was used in the end since many artifacts were produced. Although, at first glance, a visually improved image was obtained, a band histogram analysis revealed that the original pixels were slightly altered, which also affected the visual inspections to separate the four damage levels for ash. Although atmospheric correction was not absolutely necessary for the current investigations, problems of transferability of this study will arise if investigations are based on different satellite scenes or on multitemporal datasets.

Masking out shadowed tree elements was essential to minimize high in-class variance of the tree crowns, and has been recommended by e.g., [34]. Thus, focusing mainly on sunlit tree crowns greatly improved the accuracy of damage levels and tree species identification. Furthermore, since the performance of the object-based classifications strongly depends on the quality of the image segments, segmentation was iteratively optimized by empirically approximating the segments to the shapes of the tree crowns.

5.3. Reference Data

The procedure for selecting and preparing reference data samples in the framework of this study was labor-intensive and consisted of two different sources. It seems to be reliable, but some critical points need to be addressed, especially regarding the time difference between the DSW-2 records and the aerial images, and regarding the rating of the tree mortality levels. The time gap of approximately one month between the aerial images and the WV-2 orthoimage is not significant to a certain degree. Understanding the dynamics of tree mortality remains a crucial issue. Since the ash dieback is a continuous process, a narrow time-window between the reference data and the date of image acquisition might be of crucial importance. Thus, the degree of damage had to be manually checked in the aerial images by inspecting each delineated ash crown. Crown density was estimated and the resulting damage level was checked and, if necessary, adapted by experts. Since this checking and adapting of the damage level of a tree crown was done by image inspection, slight underestimation and overestimation of damages may have occurred as a consequence. Nevertheless, visual inspection is still the key for linking the on-ground traditional assessment strategies of the forest officials and the remotely sensed based approaches in many countries.

The assignment of the crown delineations to the corresponding image segments might also be a source for errors. The few mixed-pixels at crown borders, which result from e.g., bare soil, or the branches or leaves of neighboring trees with a different level of damage, may affect the corresponding image segments of a tree crown and lead to different reflectance values quite similar to those of another damage level.

Another issue is that the development of the classification method was restricted to the four different levels of damage used by the forest department, and the corresponding sample trees are stored in DSW-2. To overcome the problem of distinguishing between these different levels of tree damage, in future work, additional parameters for defining the same or other damage levels (e.g., age, general vitality, and crown diameter) should be included.

5.4. Extraction of Explanatory Variables

A key factor in this study was the use of original image bands as well as RSIs. Our results clearly demonstrated the usefulness of deriving RSIs to detect four different levels of tree damage and to a certain degree also to classify seven tree species. In this study, the implementation of adequate RSIs was based on literature research with a special focus on forests and less on agriculture, the index database and empirical testing. Three additional RSIs were developed, of which the BR (blue ratio) and GR (green–red ratio) seem particularly relevant for classifying different levels of damaged ash. Besides coastal, GNDVI, the additional RSIs GR, and RR (red ratio) are also useful for identifying tree species. The benefits of applying RSIs have been shown in several studies to detect tree stress and mortality, where most used NDVI or derivations of it, and ratios of red and green bands (e.g., [7,17,57,82]). Thus, also in this study, NIR, NDVI, RedEdge, and the green-related ratios and variables were the most important predictors for distinguishing between different damage levels. This was not the case for the tree species, for which the band ratios seemed most promising.

Since the three high-dimensional sets of explanatory variables may contain redundant information, feature extraction was applied prior to classification. In addition to stepwise variable selection methods, LDA or PCA can be used to create a set of predictors that are completely uncorrelated. These predictors can then be used as inputs to any subsequent regression model. The cross-validation of different sets of variables facilitated a straightforward interpretation of the classification models output (both species and damaged ash), tuning and performance. It indicated that principally each approach could discriminate between seven different tree species and four different levels of damaged ash, but the approach based on LDA generated the most significant models.

To reduce the large number of 66 explanatory variables, a forward and backward stepwise variable selection was run on all variables as suggested by [68,69] by testing which of the variables were significant with an error probability of <5%. Although this method is often used, it turned out to be less effective in selecting a subset of the explanatory variables for discriminating the tree species and ash damage classes. Empirical tests showed that the variables with the four highest scores seem to be most appropriate. The biggest challenge with the first approach was the handling of the large number of 66 input variables [69], as it included, for each variable, the mean, standard deviation, square of the mean, and square of the standard deviation. Stepwise procedures are straightforward and thus relatively inexpensive computationally, but they might have some drawbacks. Since standard deviations and square of the standard deviations of the explanatory variables strongly depend on the segment and pixel size (varying crown diameter) their usage might be critical and not directly transferable to datasets from other sensors. Furthermore, according to [83] problems may also be related to redundant predictors (which is possible) and the one-at-a-time nature of adding/dropping variables.

Thus, additional empirical effort was needed to assess the explanatory power of the variables and to determine a small set of powerful variables for the final classifications. Assorting the explanatory variables to different sets (e.g., [26]) is a relatively simple and straightforward method and gives an idea of the power of the variables derived from a specific sensor without performing a variable selection. To minimize the large numbers of explanatory variables of the three sets, reducing the variable space dimension by using a LDA was successfully tested. Other tree species and tree mortality classification studies (e.g., [17,25]) have also shown that a reduction of variables by LDA facilitates the straightforward interpretation of the classification model output, tuning and performance.

Reduction of variable space dimension using PCA components, which explain >95% of the variance (cumulative proportion of all components), was less effective, especially for damaged ash. Although having been widely applied for feature extraction, PCA did not produce satisfactory classification accuracies for damaged ash in this study. However, comparable high overall accuracies for tree species classification were obtained by running a PCA for feature extraction.

6. Conclusions

In conclusion, this study tested novel methods for semi-automated classification of seven tree species and four different levels of damaged ash based on explanatory variables from WV-2 original bands and RSIs. It has been shown that LDA is a very effective method for extracting the most significant features. The accuracies of the tree species classification obtained in this study are in line

with those reported in comparable studies when based only on WV-2 bands, or even higher when based on RSIs. The most significant finding is that the additionally derived RSIs have a high potential for classifying the multiple levels of tree damages affected by fungal pathogens. The overall accuracies for detecting four different levels of ash damage are promising and, according to the feedback of the forest department, also appropriate to assess the magnitude of ash dieback of the entire area.

In this approach, accurate and up-to-date information on the spatial distribution and health of tree species is provided, which is essential for forest managers. Thus, in the case of an impact, appropriate measures can be taken more effectively, also regarding future impacts such as storm events or possible insect outbreaks. For a rapid assessment of tree species diversity, the single usage of original WV-2 bands and IHS transformations would be sufficient. Regarding the overall accuracies, we expect quite comparable results when applying our methods to other regions in European forests, even if alternative high-resolution satellite data is used. Although the results are very encouraging, the developed methods have several constraints, which are listed below.

- A crucial point is the one-to-one transferability of this approach to other regions since no successful atmospheric correction was applied. Thus, robustness of the method (usage of RSIs to test classification performance) and overall accuracies might be different and likely lower.
- The performance of an object-based classification depends on the quality of the segments, *i.e.*, their approximation to the real tree crowns or parts of them. Thus, using additional 3D data from digital surface models may further improve the segmentation of tree crowns. Automatic individual tree crown delineation, as successfully applied in many studies, should also be further investigated.
- Since the derivation of RSI is time consuming, simply using WV-2 bands and the band ratios to classify species is an efficient alternative. To distinguish different levels of damaged ash, alternative sensors, e.g., ALS or hyperspectral datasets should be tested. Possible modification of the signatures due to the pan-sharpening should be investigated as well.
- To further improve the distinction between different levels of damaged ash or trees in general, the time gap between the collection of reference data and acquisition of images should be minimized to few weeks. Acquiring multitemporal imagery (e.g., yearly) from other high-resolution spaceborne sensors should also be considered. Another improvement could be to use a continuous approach, *i.e.*, to give the probabilities of a damage level per crown or to predict the decline of foliage on a continuous scale (0–100%). Future work may also include the assessment of biophysical parameters based on image spectroscopy as suggested e.g., in [20,21].
- The usage of an independent reference dataset should be considered when applying on larger datasets, e.g., on the State level.

Overcoming these constraints will underscore the advantages of satellite-based approaches (large area coverage, less processing and operator interaction, more spectral information) and help to reduce the collection of costly a-priori information (reference data sampling and additional acquisition of aerial imagery).

Acknowledgments

The study was carried out in collaboration between the state forest Mecklenburg–Vorpommern, Department of Forest Planning, Lab Practice, and Information Systems, with the Remote Sensing Group of the Swiss Federal Research Institute WSL. It was funded by the State Forest Department Mecklenburg–Vorpommern, the Swiss Federal Research Institute WSL and by the European Commission in the framework of the INTERREG project "Development of trans-border decision support system for remote sensing and model assessment of forest dendromass in Pomerania Region" (INT-09-0039). We are grateful to Silvia Dingwall for the English revision of the manuscript, to Achilleas Psomas, our in-house expert for spaceborne remote sensing, for fruitful discussions while preparing the manuscript.

Author Contributions

Lars T. Waser led the study, performed tree species and damaged ash classifications and wrote the manuscript. Kai Jütte provided and processed the WV-2 imagery and coordinated reference data collection. Theresia Stampfer processed and analysed remote sensing indices and provided several figures. Meinrad Küchler contributed in statistical support and R programming.

Conflicts of Interest

The authors declare no conflict of interest.

References

1. Allen, C.D.; Macalady, A.K.; Chenchouni, H.; Bachelet, D.; McDowell, N.; Vennetier, M.; Kitzberger, T.; Rigling, A.; Breshears, D.D.; Hogg, E.H.; *et al.* A global overview of drought and heat-induced tree mortality reveals emerging climate change risks for forests. *For. Ecol. Manag.* **2010**, *259*, 660–684.
2. Jönsson, A.M.; Appelberg, G.; Harding, S.; Bärring, L. Spatio-temporal impact of climate change on the activity and voltinism of the spruce bark beetle Ips. typographus. *Glob. Chang. Biol.* **2009**, *15*, 486–499.
3. Gross, A.; Zaffarano, P.L.; Grünig, C.R. Reproductive mode and life cycle of the ash dieback pathogen *Hymenoscyphus pseudoalbidus*. *Fungal Genet. Biol.* **2012**, *49*, 977–986.
4. Meddens, A.J.H.; Hicke, J.A.; Vierling, L.A.; Hudak, A.T. Evaluating methods to detect bark beetle-caused tree mortality using single-date and multi-date Landsat imagery. *Remote Sens. Environ.* **2013**, *132*, 49–58.
5. Honkavaara, E.; Litkey, P.; Nurminen, K. Automatic storm damage detection in forests using high-altitude photogrammetric imagery. *Remote Sens.* **2013**, *5*, 1405–1424.
6. Eitel, J.U.H.; Vierling, L.A.; Litvak, M.E.; Long, D.S.; Schulthess, U.; Ager, A.A.; Krofcheck, D.J.; Stoscheck, L. Broadband, red-edge information from satellites improves early stress detection in a New Mexico conifer woodland. *Remote Sens. Environ.* **2011**, *115*, 3640–3646.

7. Coops, N.C.; Johnson, M.; Wulder, M.A.; White, J.C. Assessment of QuickBird high spatial resolution imagery to detect red attack damage due to mountain pine beetle infestation. *Remote Sens. Environ.* **2006**, *103*, 67–80.
8. Hicke, J.A.; Logan, J. Mapping white bark pine mortality caused by a mountain pine beetle outbreak with high spatial resolution satellite imagery. *Int. J. Remote Sens.* **2009**, *30*, 4427–4441.
9. Wulder, M.A.; White, J.C.; Coops, N.C.; Butson, C.R. Multi-temporal analysis of high spatial resolution imagery for disturbance monitoring. *Remote Sens. Environ.* **2008**, *112*, 2729–2740.
10. White, J.C.; Wulder, M.A.; Brooks, D.; Reich, R.; Wheate, R.D. Detection of red attack stage mountain pine beetle infestation with high spatial resolution satellite imagery. *Remote Sens. Environ.* **2005**, *96*, 340–351.
11. Kim, Y.; Yang, Z.; Cohen, W.B.; Lauver, C.L.; Vankat, J.L. Distinguishing between live and dead standing tree biomass on the North Rim of Grand Canyon National Park, USA using small-footprint lidar data. *Remote Sens. Environ.* **2009**, *113*, 2499–2510.
12. Vastaranta, M.; Kantola, T.; Lyytikäinen-Saarenmaa, P.; Holopainen, M.; Kankare, V.; Wulder, M. Area-based mapping of defoliation of scots pine stands using airborne scanning LiDAR. *Remote Sens.* **2013**, *5*, 1220–1234.
13. Coops, N.C.; Varhola, A.; Bater, C.W.; Teti, P.; Boon, S.; Goodwin, N.; Weiler, M. Assessing differences in tree and stand structure following beetle infestation using lidar data. *Can. J. Remote Sens.* **2009**, *35*, 497–508.
14. Frolking, S.; Palace, M.W.; Clark, D.B.; Chambers, J.Q.; Shugart, H.H.; Hurtt, G.C. Forest disturbance and recovery: A general review in the context of spaceborne remote sensing of impacts on aboveground biomass and canopy structure. *J. Geophys. Res.* **2009**, *114*, 1–27.
15. Pontius, J.; Martin, M.; Plourde, L.; Hallett, R. Ash decline assessment in emerald ash borer-infested regions: A test of tree-level, hyperspectral technologies. *Remote Sens. Environ.* **2008**, *112*, 2665–2676.
16. Fassnacht, F.E.; Latifi, H.; Ghosh, A.; Joshi, P.K.; Koch, B. Assessing the potential of hyperspectral imagery to map bark beetle-induced tree mortality. *Remote Sens. Environ.* **2014**, *140*, 533–548.
17. Garrity, S.R.; Allen, C.D.; Brumby, S.P.; Gangodagamage, C.; McDowell, N.G.; Cai, D.M. Quantifying tree mortality in a mixed species woodland using multitemporal high spatial resolution satellite imagery. *Remote Sens. Environ.* **2013**, *129*, 54–65.
18. Wulder, M.A.; Dymond, C.C.; White, J.C.; Leckie, D.G.; Carroll, A.L. Surveying mountain pine beetle damage of forests: A review of remote sensing opportunities. *For. Ecol. Manag.* **2006**, *221*, 27–41.
19. Skakun, R.S.; Wulder, M.A.; Franklin, S.E. Sensitivity of the thematic mapper enhanced wetness difference index to detect mountain pine beetle red-attack damage. *Remote Sens. Environ.* **2003**, *86*, 433–443.
20. Carleer, A.; Wolff, E. Exploition of very high resolution satellite data for tree species identification. *Photogramm. Eng. Remote Sens.* **2004**, *70*, 135–140.
21. Schlerf, M.; Atzberger, C.; Hill, J. Remote sensing of forest biophysical variables using HyMap imaging spectrometer data. *Remote Sens. Environ.* **2005**, *95*, 177–194.

22. Schlerf, M.; Atzberger, C.; Hill, J.; Buddenbaum, H.; Werner, W.; Schüler, G. Retrieval of chlorophyll and nitrogen in Norway spruce (*Picea. abies* L. Karst.) using imaging spectroscopy. *Int. J. Appl. Earth Obs.* **2010**, *12*, 17–26.
23. Chen, Q. *Comparison of WorldView-2 and IKONOS-2 Imagery for Identifying Tree Species in the Habitat of an Endangered Bird Species in Hawaii 8-Band Research Challenge*; Digital Globe: Longmont, CO, USA, 2011.
24. Stoffels, J.; Mader, S.; Hill, J.; Werner, W.; Ontrup, G. Satellite-based stand-wise forest cover type mapping using a spatially adaptive classification approach. *Eur. J. For. Res.* 2012, 131, 1071–1089.
25. Immitzer, M.; Atzberger, C.; Koukal, T. Tree species classification with random forest using very high spatial resolution 8-Band WorldView-2 satellite data. *Remote Sens.* **2012**, *4*, 2661–2693.
26. Waser, L.T.; Ginzler, C.; Kuechler, M.; Baltsavias, E.; Hurni, L. Semi-automatic classification of tree species in different forest ecosystems by spectral and geometric variables derived from Airborne Digital Sensor (ADS40) and RC30 data. *Remote Sens. Environ.* **2011**, *115*, 76–85.
27. Leckie, D.G.; Tinis, S.; Nelson, T.; Burnett, C.H.; Gougeon, F.A.; Cloney, E.; Paradine, D. Issues in species classification of trees in old growth conifer stands. *Can. J. Remote Sens.* **2005**, *31*, 175–190.
28. Kim, S.; McGaughey, R.J.; Andersen, H.E.; Schreuder, G. Tree species differentiation using intensity data derived from leaf-on and leaf-off airborne laser scanner data. *Remote Sens. Environ.* **2009**, *113*, 1575–1586.
29. Heinzel, J.N.; Koch, B. Exploring full-waveform LiDAR parameters for tree species classification. *Int. J. Appl. Earth Obs. Geoinf.* **2011**, *13*, 152–160.
30. Marchisio, G.; Pacifici, F.; Padwick, C. On the Relative Predictive Value of the New Spectral Bands in the Worldwiew-2 Sensor. In Proceedings of 2010 IEEE International Geoscience and Remote Sensing Symposium (IGARSS), Honolulu, HI, USA, 25–30 July 2010; pp. 2723–2726.
31. Digital Globe. *White Paper: The Benefits of the 8 Spectral Bands of WorldView-2*; Digital Globe: Longmont, CO, USA, 2009.
32. Gwata, B. Developing high resolution clutter for wireless network propagation using WorldView-2 imagery. *Proc. SPIE* **2012**, *8390*, doi:10.1117/12.919091
33. Omar, H. *Commercial Timber Tree Species Identification Using Multispectral WorldView-2 Data, 8-Band Research Challenge*; Digital Globe: Longmont, CO, USA, 2011.
34. Pu, R.; Landry, S.A. Comparative analysis of high spatial resolution IKONOS and WorldView-2 imagery for mapping urban tree species. *Remote. Sens. Environ.* **2012**, *124*, 516–533.
35. Riggan, N.D., Jr.; Weih, R.C., Jr. A Comparison of Pixel-based versus object-based land use/land cover classification methodologies. *J. Ark. Acad. Sci.* **2009**, *63*, 145–152.
36. Whiteside, T.G.; Boggs, G.S.; Maier, S.W. Comparing object-based and pixel-based classifications for mapping savannas. *Int. J. Appl. Earth Obs.* **2011**, *13*, 884–893.
37. Ju, J.; Kolaczyk, E.D.; Gopal, S. Gaussian mixture discriminant analysis and sub-pixel land cover characterization in remote sensing. *Remote Sens. Environ.* **2003**, *84*, 550–560.
38. Guisan, A.; Edwards, T.E.; Hastie, T. Generalized linear and generalized additive models in studies of species distributions: Setting the scene. *Ecol. Model.* **2002**, *157*, 89–100.
39. Duda, R.O.; Hart, P.E.; Stork, D.G. *Pattern Classification*, 2nd ed.; John Wiley & Sons: New York, NY, USA, 2000.

40. Chavez, P.S., Jr.; Sides, S.C.; Anderson, A. Comparison of three different methods to merge multiresolution and multispectral data: Landsat TM and SPOT Panchromatic. *Photogramm. Eng. Remote Sense.* **1991**, *57*, 295–303.
41. Bakys, R.; Vasaitis, R.; Barklund, P.; Ihrmark, K.; Stenlid, J. Investigations concerning the role of *Chalara fraxinea* in declining *Fraxinus excelsior*. *Plant Pathol.* **2009**, *58*, 284–292.
42. Multiresolution Segmentation—An Optimization Approach for High Quality Multi-Scale Image Segmentation. Available online: http://www.isprs.org/proceedings/xxxviii/4-c7/pdf/Happ_143.pdf (accessed on 12 March 2014).
43. Benz, U.; Hofmann, P.; Willhauck, G.; Lingenfelder, I.; Heynen, M. Multi-resolution, object-oriented fuzzy analysis of remote sensing data for GIS-ready information. *ISPRS J. Photogramm.* **2004**, *58*, 239–258.
44. Gonzales, R.C.; Woods, R.E. *Digital Image Processing*, 2nd ed.; Prentice Hall: New York, NY, USA, 2000.
45. Schowengerdt, R.E. *Remote Sensing: Models and Methods for Image Processing*; Academic Press and Elsevier: Amsterdam, The Nederlands, 2006.
46. Yu, Q.; Gong, P.; Clinton, N.; Biging, G.; Kelly, M.; Schirokauer, D. Object-based detailed vegetation classification with airborne high spatial resolution remote sensing imagery. *Photogramm. Eng. Remote Sense.* **2006**, *72*, 799–811.
47. Waser, L.T. Airborne Remote Sensing Data for Semi-Automated Extraction of Tree Area and Classification of Tree Species. Ph.D. Dissertation 20464, Swiss Federal Institute of Technology-ETH Zurich, 2012. Available online: http://e-collection.library.ethz.ch/view/eth:6087 (accessed on 12 March 2014).
48. Bannari, A.; Morin, D.; Huette, A.R.; Bonn, F.A. A review of vegetation indices. *Remote. Sens. Environ.* **1995**, *13*, 95–120.
49. Jackson, R.D.; Huete, A.R. Interpreting vegetation indices. *Prev. Vet. Med*. **1991**, 11, 185–200.
50. Gitelson, A.A.; Kaufman, Y.; Merzlyak, M.N. Use of green channel in remote sensing of global vegetation from EOS-MODIS. *Remote Sens. Environ.* **1996**, *58*, 289–298.
51. Vogelmann, J.E.; Rock, B.N.; Moss, D.M. Red edge spectral measurements from sugar maple leaves. *Int. J. Remote Sens.* **1993**, *14*, 1563–1575.
52. Haboudane, D.; Miller, J.R.; Pattey, E.; Zarco-Tejada, P.; Strachan, I.B. Hyperspectral vegetation indices and novel algorithms for predicting green LAI of crop canopies: Modeling and validation in the context of precision agriculture. *Remote. Sens. Environ.* **2004**, *90*, 337–352.
53. ENVI, 2013. Available online: http://www.exelisvis.com/docs/VegetationIndices.html (accessed on 10 April 2014).
54. Index Database, 2013. Available online: http://www.indexdatabase.de/ (accessed on 10 April 2014).
55. Cyperski, J. Untersuchung von Filtern zur Aufnahme von IR-Luftbildern für die Forstwirtschaft. Bachelor Thesis, Beuth Hochschule für Technik Berlin, Berlin, Germany, 10 April 2012; pp. 1–40.
56. Kaufman, Y.J.; Tanré, D. Atmospherically resistant vegetation index (ARVI) for EOS-MODIS. *IEEE Trans. Geosci. Remote Sens.* **1992**, *30*, 261–270.

57. Filchev, L. An Assessment of European Spruce Bark Beetle Infestation Using WorldView-2 Satellite Data. In Proceedings of 1st European SCGIS Conference with International Participation "Best Practices: Application of GIS Technologies for Conservation of Natural and Cultural Heritage Sites" (SCGIS-Bulgaria, Sofia), Sofia, Bulgaria, 21–23 May 2012; pp. 9–16.
58. Hildebrandt, G. *Fernerkundung und Luftbildmessung für Forstwirtschaft, Vegetationskartierung und Landschaftsökologie*; Herbert Wichmann Verlag: Heidelberg, Germany, 1996.
59. Le Maire, G.; Francois, C.; Dufrene, E. Towards universal broad leaf chlorophyll indices using PROSPECT simulated database and hyperspectral reflectance measurements. *Remote Sens. Environ.* **2004**, *89*, 1–28.
60. Ahamed, T.; Tian, L.; Zhang, Y.; Ting, K.C. A review of remote sensing methods for biomass feedstock production. *Biomass Bioenerg.* **2011**, *35*, 2455–2469.
61. Viña, A.; Gitelson, A.A. New developments in the remote estimation of the fraction of absorbed photosynthetically active radiation in crops. *Geophys. Res. Lett.* **2005**, *32*, 1–4.
62. Sims, D.A.; Gamon, J.A. Relationships between leaf pigment content and spectral reflectance across a wide range of species, leaf structures and developmental stages. *Remote Sens. Environ.* **2002**, *81*, 337–354.
63. Salifu, T.; Agyare, W.A. Distinguishing land use types using surface albedo and normalized difference vegetation index derived from the SEBAL model for the Atankwidi and Afram subcatchments in Ghana. *J. Eng. Appl. Sci.* **2012**, *7*, 69–80.
64. Walz, U.; Hou, W. Charakterisierung der Landschaftsvielfalt mit RapidEye-Daten—Erste Ergebnisse und Erfahrungen. In *RapidEye Science Archive (RESA)—Erste Ergebnisse, Proceedings of the 3*; RESA Workshop: Erik Borg, Holger Daedelow (Hrsg.), 2011; pp. 75–85.
65. Chávez, R.; Clevers, J.G.P.W. Phase 2. In *Object-Based Analysis of 8-Bands WorldView-2 Imagery for Assessing Health Condition of Desert Trees, 8-Band Research Challenge*; Digital Globe: Longmont, CO, USA, 2011; pp. 1–8.
66. Latifi, H.; Nothdurft, A.; Koch, B. Non-parametric prediction and mapping of standing timber volume and biomass in a temperate forest: Application of multiple optical/LiDAR-derived predictors. *Forestry* **2010**, *83*, 395–407.
67. Guisan, A.; Weiss, S.B.; Weiss, A.D. GLM *versus* CCA spatial modeling of plant species distribution. *Plant Ecol.* **2004**, *143*, 107–122.
68. Hosmer, D.W.; Lemeshow, S. *Applied Logistic Regression*, 2nd ed.; Wiley: New York, NY, USA, 2000.
69. Akaike, H. Information Theory as an Extension of the Maximum Likelihood Principle. In Proceedings of the 2nd International Symposium on Information Theory, Budapest, Hungary, 9–13 June 2013; Petrov, B.N., Csaki, F., Eds.; Akademiai Kiado: Budapest, Hungary, pp. 267−281.
70. R Statistics. 2013. Available online: http://cran.r-project.org/manuals.html (accessed on 10 April 2014).
71. VEGEDAZ. 2014. VEGADAZ Software Version 2014. Available online: http://www.wsl.ch/dienstleistungen/produkte/software/vegedaz/index_EN (accessed on 10 April 2014).
72. Fukunaga, K. *Introduction to Statistical Pattern Recognition*, 2nd ed.; Academic Press: New York, NY, USA, 1990.

73. Everitt, B.S.; Dunn, G. *Applied Multivariate Data Analysis*; Arnold Publisher: London, UK, 2001.
74. Swan, A.R.H.; Sandilands, M. *Introduction to Geological Data Analysis*; Blackwell Science: Oxford, UK, 1995.
75. Venables, W.N.; Ripley, B.D. *Modern Applied Statistics with S*, 4th ed.; Springer: New York, NY, USA, 2002.
76. Cohen, J. A coefficient of agreement for nominal scales. *Educ. Psychol. Meas.* **1960**, *20*, 37–46.
77. Richter, K.; Atzberger, C.; Hank, T.B.; Mauser, W. Derivation of biophysical variables from earth observation data: Validation and statistical measures. *J. Appl. Remote Sens.* **2012**, *6*, doi:10.1117/1.JRS.6.063557.
78. Shao, J. Linear model selection by cross-validation. *J. Am. Stat. Assoc.* **1993**, *88*, 486–494.
79. Efron, B. Estimating the error rate of a prediction rule: Improvement on cross-validation. *J. Am. Statist. Assoc.* **1983**, *78*, 316–331.
80. Hollander, M.; Wolfe, D.A. *Nonparametric Statistical Methods*, 2nd ed.; Wiley: New York, NY, USA, 1999.
81. Kim, S.R.; Lee, W.K.; Kwak, D.A.; Biging, G.S.; Gong, P.; Lee, J.H.; Cho, H.K. Forest cover classification by optimal segmentation of high resolution satellite imagery. *Sensors* **2011**, *11*, 1943–1958.
82. Meddens, A.J.H.; Hicke, J.A.; Vierling, L.A. Evaluating the potential of multispectral imagery to map multiple stages of tree mortality. *Remote Sens. Environ.* **2011**, *115*, 1632–1642.
83. Brauner, N.; Shacham, M. Role of range and precision of the independent variable in regression of data. *J. Am. Inst. Chem. Eng.* **1998**, *44*, 603–611.

Appendix

In the first variable selection approach, both the forward and backward stepwise selection algorithm (R module *stats*) was run on the 33 explanatory variables (66 means and standard deviations of them) to separate the significant from non-significant variables. How often each explanatory variable was selected automatically was then counted.

Table A1 shows how in the tree species classification, the four highest scores (9, 8, 7, 6) of the stepwise selected variables were obtained for the variables: 9 (coastal, GNDVI, GR, RR), 8 (NDRE, NORM NIR), 7 ($I_{[RGB],}$ $I_{[RGNIR1]}$, $NDVI_{8,4,}$ REY), and 6 (RedEdge, $H_{[RGB],}$ DD, NDVI).

Table A2 shows how, in the classification of damaged ash, the three highest scores (6, 5, 4) of the stepwise selected variables were obtained for the variables: 6 (REY, BR), 5 (ARVI, GNDVI, GR), and 4 (yellow, GI2, NDVI, RR).

Table A3 shows the proportions of trace for the discriminant scores (six for the tree species and three for the ash damages) obtained by the LDAs. The first trace number indicates the percentage of between-group variance that the first discriminant function is able to explain from the total amount of between-group variance. All linear discriminants were used to assess the predictive power of the new classification models (see Tables 5 and 7).

For the tree species classification based on all 33 explanatory variables (66 means and standard deviations of them), standard deviation (σ), proportion of variance (PV), and cumulative proportion (CP) of the first eight PCA components are shown in Table A4. The PCAs which explain >95% of the

variance (PCA axes 1–7) were used to assess the predictive power of a new classification model (see Table 5).

For the classification of ash damage levels based on all 33 explanatory variables (66 means and standard deviations of them), standard deviation (σ), proportion of variance (PV), and cumulative proportion (CP) of the first eleven PCA components are shown in Table A5. The PCAs which explain >95% of the variance (PCA axes 1–7) were used to assess the predictive power of a new classification model (see Table 7).

Table A1. Overview of the selected variables for the tree species classification. For each tree species, the number of variables (mean and standard deviation) from the stepwise selection are given. (--) are the non-significant or the non-selected. The total counts per variable is given in the last columns.

		Tree Species							
	Variable	**Ash**	**Beech**	**Douglas Fir**	**Larch**	**Norway Spruce**	**Oak**	**Poplar**	**Total**
WV-2 Image Bands	coastal	2	2	1	--	--	2	2	**9**
	blue	--	1	--	--	--	1	1	3
	green	1	2	--	--	--	--	--	3
	yellow	1	--	--	--	--	1	--	2
	red	1	1	--	--	--	--	--	2
	RedEdge	2	--	1	--	1	1	1	**6**
	NIR1	1	1	--	--	--	--	1	3
	NIR2	1	--	--	--	--	1	1	3
	$I_{[RGB]}$	2	2	--	--	--	1	2	**7**
	$H_{[RGB]}$	1	2	--	--	--	2	1	**6**
	$S_{[RGB]}$	1	1	--	--	--	1	--	3
	$I_{[RGNIR1]}$	1	1	1	--	1	1	2	**7**
	$H_{[RGNIR1]}$	1	2	--	--	--	1	--	4
	$S_{[RGNIR1]}$	1	1	--	--	--	1	1	4
Remote Sensing Indices	ARVI	--	1	--	--	--	--	--	1
	DD	1	1	1	--	--	1	2	**6**
	GI2	2	--	--	--	--	1	--	3
	GNDVI	2	2	1	--	--	2	2	**9**
	NDRE	2	1	1	--	1	1	2	**8**
	NDVI	2	--	--	--	1	1	2	**6**
	$NDVI_{3,5}$	1	--	--	--	1	2	--	4
	$NDVI_{8,4}$	2	2	--	--	--	2	1	**7**
	NIRRY	1	1	--	--	--	--	1	3
	NORM NIR	2	2	1	--	--	2	1	**8**
	PSRI	1	1	--	--	--	--	2	4
	REY	2	1	1	--	--	2	1	**7**
	RVI	1	1	--	--	--	1	1	4
	SA	1	1	--	--	--	1	1	4
	VI1	1	1	--	--	--	1	--	3
	VIRE	--	--	--	--	--	--	1	1
	BR	1	1	--	--	--	1	--	3
	GR	2	2	--	--	1	2	2	**9**
	RR	2	2	1	--	1	1	2	**9**

Table A2. Overview of the selected variables for the classification of damaged ash. For each damage level, the number of variables (mean and standard deviation) from the stepwise selection are given. (--) are the non-significant or the non-selected. The total counts per variable is given in the two last columns.

Damaged Ash						
Variable		**Level 1**	**Level 2**	**Level 3**	**Level 4**	**Total**
WV-2 Image Bands	coastal	--	--	--	--	0
	blue	--	1	1	1	3
	green	--	--	--	--	0
	yellow	1	1	1	1	**4**
	red	1	--	--	1	2
	RedEdge	--	--	--	2	2
	NIR1	--	--	1	--	1
	NIR2	--	--	--	--	0
	$I_{[RGB]}$	1	1	1	--	3
	$H_{[RGB]}$	--	--	--	--	0
	$S_{[RGB]}$	1	--	--	--	1
	$I_{[RGNIR1]}$	1	1	--	1	3
	$H_{[RGNIR1]}$	--	--	1	--	1
	$S_{[RGNIR1]}$	--	--	--	--	0
Remote Sensing Indices	ARVI	1	2	1	1	**5**
	DD	1	--	--	1	2
	GI2	1	--	1	2	**4**
	GNDVI	1	1	1	2	**5**
	NDRE	1	--	1	1	**3**
	NDVI	1	1	1	1	**4**
	$NDVI_{3,5}$	2	--	1	--	3
	$NDVI_{8,4}$	1	--	1	1	3
	NIRRY	1	1	--	1	3
	NORM NIR	1	--	1	--	2
	PSRI	1	--	--	--	1
	REY	2	2	1	1	**6**
	RVI	1	--	--	--	1
	SA	1	--	1	1	2
	VI1	--	--	1	1	2
	VIRE	1	--	--	1	2
	BR	2	1	1	2	**6**
	GR	2	1	2	--	**5**
	RR	1	1	2	--	**4**

Table A3. Overview of the proportion of trace obtained by the LDAs based on all 33 explanatory variables (66 means and standard deviations of them).

	LD1	**LD2**	**LD3**	**LD4**	**LD5**	**LD6**
Tree Species	0.891	0.056	0.041	0.009	0.003	0.001
Damaged Ash	0.872	0.089	0.038	--	--	--

Table A4. Overview of the first eight PCA components used for the classification of tree species. The measures are: standard deviation (σ), proportion of variance (PV), and cumulative proportion (CP).

Tree Species	**PCA Components**							
	PC1	PC2	PC3	PC4	PC5	PC6	PC7	PC8
σ	4.44	3.32	2.84	1.73	1.40	1.09	0.82	0.69
PV	0.41	0.23	0.17	0.06	0.04	0.03	0.01	0.01
CP	0.41	0.64	0.81	0.87	0.91	0.94	0.95	0.96

Table A5. Overview of the first eight PCA components used for the classification of damaged ash. The measures are: standard deviation (σ), proportion of variance (PV), and cumulative proportion (CP).

Damaged Ash	**PCA Components**							
	PC1	PC2	PC3	PC4	PC5	PC6	PC7	PC8
σ	4.58	3.57	2.26	1.67	1.39	1.03	0.89	0.82
PV	0.44	0.26	0.11	0.06	0.04	0.02	0.02	0.01
CP	0.44	0.70	0.81	0.87	0.91	0.93	0.95	0.96